

## Chapter II

# Fluid Statics and Capillarity

I. Martinez \*, J.M. Haynes \*\*, D. Langbein \*\*\*

Large, curved and quiescent fluid interfaces can only be realized under microgravity conditions. This enables one to investigate macroscopic, partly contained fluids having high sensitivity to weak forces. Capillary equilibrium and stability, wetting, convection driven by interfacial tension gradients, the influence of centrifugal, electric and magnetic forces normally overruled by gravity can be studied in detail.

Following a general treatment of interface properties on the molecular level, the Gibbs model of interfaces is discussed. Recent results of microgravity investigations on capillary stability and wetting are reported. Finally, the prospects for future activities are discussed. The examples considered are: dynamics of wetting, foam stability and study of intermolecular forces with implications for crystal growth, preparation of composite materials and immiscible alloys.

### A. Introduction

Technological interest in the behaviour of liquids in low gravity extends back over two centuries, to the first use of a drop-tower for production of spherical lead shot [1]. By the mid-19th century, more fundamental interest was already intensive when Plateau [2] and others pioneered the use of the neutral buoyancy technique for the study of capillary phenomena free from the primary influence of gravity.

More recently, the availability of advanced drop-tower facilities, of parabolic trajectories in aircraft and sounding rockets, and above all of manned orbital flight, has facilitated development in the field. Largely, this has been driven by the same motives as those of the two historical examples cited above: interests in materials processing and in fundamental studies of capillary phenomena. A third driver has more to do with orbital flight per se: the need to understand and control the location and the motion of liquid propellants in orbiting vehicles.

As regards the first of these, the original motivation was provided by the prospect of commercial materials processing in microgravity. While it is clear that a more cautious view of this possibility prevails nowadays, interest is sustained by the belief that such studies can lead to a deeper understanding of terrestrial processes. Meanwhile, more basic studies of capillarity have moved towards increasingly complex phenomena, often involving dynamics and therefore covered mainly in Chapter III.

---

\* E.T.S.I. Aeronauticos, Ciudad Universitaria, 28040 Madrid, Spain

\*\* University of Bristol, School of Chemistry,  
Cantock's Close, BS8 ITS Bristol, England

\*\*\* Battelle Institut, Am Römerhof 35, 6000 Frankfurt am Main 90, West-Germany

Here, we shall first briefly review the relevant basic physics, merely to underline those phenomena where low-gravity conditions are advantageous. Extensive theoretical advances have been made in this field during the last decade, prompted by the advent of opportunities for space experimentation. We shall then describe the results of selected experiments on fluid statics and capillarity which have already been conducted in microgravity, and go on to give our view of what future experiments could – or should – accomplish. This scheme introduces an arbitrary distinction between what was known in the early 1970's and what has been discovered since. In retrospect, however, it will be seen that it was the practical realization of microgravity conditions for fluid physics experiments that provided a watershed, which has spawned numerous theoretical and experimental advances.

## B. Basic Physics

### B.1. Influence of Gravity

At the molecular level, gravity is a weak body force,  $10^{40}$  times smaller than the electrostatic force in the hydrogen atom, and  $10^{35}$  times smaller than that in the molecule of hydrogen. Thus, properties controlled by intermolecular forces (such as surface tension, contact angle and fluid miscibility) are expected to be sensibly independent of gravity <sup>1</sup>. On the other hand, gravity forces accumulate and become dominant when large masses are present, unless balanced by another body force; thus, removal of gravity effects enhances the susceptibility of large fluid masses to small force fields. The main advantage that microgravity offers to fluid science is therefore the possibility of achieving *large quiescent interfaces, of uniform mean curvature, free from gradients of hydrostatic pressure, and showing high sensitivity to weak forces.*

The relative influence of capillary and gravitational forces is expressed by the dimensionless Bond number:

$$Bo = \Delta\rho g d^2 / \sigma \quad (1)$$

where  $\sigma$  = interfacial tension between two fluid phases,  
 $d$  = a characteristic dimension,  
 $\Delta\rho$  = density difference between two fluid phases, and  
 $g$  = gravitational acceleration.

The capillary length,  $l$ , given by:

$$l = (\sigma / g \Delta\rho)^{1/2} \quad (2)$$

is often used to non-dimensionalize descriptions of interface shape; thus, the Bond number can also be written as:

<sup>1</sup> For a dissenting view regarding contact angle, see A.W. Adamson, "Physical Chemistry of Surfaces", 3rd edition, Wiley, 1976, p.358

$$Bo = d^2/l^2 \quad (3)$$

The static behaviour of a body of fluid is therefore dominated by capillary forces if any of  $d$ ,  $\Delta\rho$  or  $g$  is small (large  $\sigma$  values cannot be realized). The case of small  $d$  presents practical difficulties. That of small  $\Delta\rho$  was the province of Plateau. The case of small  $g$  is our present concern. It should be remarked that Plateau's approach, while inexpensive, has limitations where dynamic phenomena are concerned, or where control of the fluid/fluid/solid contact angle is necessary.

Experiments have therefore concentrated on those phenomena which, while normally overwhelmed by terrestrial gravity, become dominant when gravity is reduced. These include problems of capillary equilibrium and stability, of wetting, and of convective phenomena driven by gradients of surface tension, of electric potential and of centrifugal force, that are normally hidden by the operation of terrestrial gravity. These are of interest both fundamentally and because of their relevance to materials processing.

## B.2. Macroscopic and Microscopic Views of the Interface

Capillary phenomena provide a visible and macroscopic demonstration of the existence of intermolecular forces, which operate on a scale beyond the limits of direct experimental observation. For this reason, they have excited interest for almost 300 years. Their understanding progressed substantially in the second half of the 19th century, when the molecular-kinetic view of matter was elaborated.

The application of pure classical thermodynamics to the fluid interface is necessarily limited to descriptions of macroscopic phenomena, since it can deal only with volume-elements large enough to contain sufficient molecules for their positional and energy distributions to be considered statistically uniform and homogeneous. This immediately rules out detailed thermodynamic examination of the interface itself, where the densities of matter, energy and entropy vary rapidly over distances of the order of the range of intermolecular forces. This difficulty was circumvented by the conceptual model of Gibbs [3], in which the physical interface was replaced by a dividing surface of strictly zero thickness, on either side of which the bulk phases were supposed to have perfectly uniform densities of matter, energy and entropy. Any discrepancies in the total amounts of these quantities between model and real systems were then assigned to the dividing surface itself, and defined as surface excesses (or deficits) per unit area. The resultant thermodynamics will be summarized briefly in Section B.3. Gross thermodynamic properties such as surface tension, surface energy and surface mass excess are fully included in such a model, but the interfacial structure remains entirely unknown.

Many attempts have been made to extend this treatment to include a more detailed view of the microscopically inhomogeneous region close to the interface, by the device of local thermodynamics. In the simplest version of this, local densities are assumed to be smooth functions of the co-ordinate normal to the surface, and to contribute to the total energy in their normal (i.e. linear) way, as in bulk thermodynamics. This, however, predicts a density

profile of infinitesimal gradient and an interface of infinite thickness, having zero interfacial tension. Van der Waals [4] overcame this by adding an energy term proportional to the square of the density gradient; this succeeds in predicting a non-zero interfacial tension, but leaves unanswered the question of whether other even powers of the gradient (or of higher density-derivatives) should be included. Furthermore, all such treatments rest on the possibly hazardous assumption that thermodynamic functions can properly be defined locally in a microscopically inhomogeneous fluid.

A rather more profitable approach has been the use of statistical mechanical methods to calculate the molecular distribution (and/or correlation) functions, as a function of position within the inhomogeneous region. This yields analytical expressions for the equilibrium density profile across the interface, from which the interfacial tension may be calculated with reasonable success. However, consideration of permitted density fluctuations within such a theory leads to the disturbing conclusion that, in the absence of gravity or some other such stabilizing field, the thickness and structure of the interface become indeterminate. This notion is, of course, not only intuitively unreasonable, but also contradicts extensive experience accumulated in microgravity. The difficulty has recently been at least partially rationalized [5].

Computer simulation of the microstructure of fluid interfaces is feasible, using either molecular dynamics or Monte Carlo methods, though even the most powerful machines are at present limited to assemblies of about  $10^3$  molecules. Nevertheless, such "experiments" have led to estimates of surface tension, as a function of temperature, for simple fluids (such as argon), which agree very well with laboratory measurements. As with statistical mechanical calculations, the results depend on the form of the intermolecular potential that is inserted in the model. Confidence in the method is such that there is a discernible tendency to use the results to discriminate between alternative potential functions.

Although the topics mentioned in this section have generated a very extensive literature, we have cited few references, since the whole subject has recently been comprehensively reviewed [6].

### B.3. Thermodynamics of the Gibbs Model

Consider a closed system comprising two fluid phases separated by an interface, containing  $i$  non-reacting chemical components, and not subject to any external force field. For equilibrium, the total entropy must be maximized. Thus (using superscripts ' and '' to label the two bulk phases, and superscript  $\sigma$  for the interface):

$$S = S' + S'' + S^\sigma = \text{maximum} \quad (4)$$

subject to the constraints of constant volume  $V$ , energy  $U$ , and number of moles of each component  $n_i$ . In the Gibbs model, the interface has no volume, so:

$$V = V' + V'' + 0 = \text{constant} \quad \text{and} \quad (5)$$

$$U = U' + U'' + U^\sigma = \text{constant} \quad (6)$$

$$n_i = n_i' + n_i'' + n_i^\sigma = \text{constant, for all } i \quad (7)$$

Substitution into eq. (4) of  $dS = (1/T)dU + (p/T)dV - \sum(\mu_i/T)dn_i$  for each bulk phase, and  $dS = (1/T)dU - (\sigma/T)dA^\sigma - \sum(\mu_i/T)dn_i$  for the interface, where  $\mu_i$  is the chemical potential of the  $i$ -th component, together with eq. (5) - (7), yields:

$$T' = T'' = T^\sigma \quad (8)$$

$$p' = p'' + \sigma dA^\sigma/dV' \quad (9)$$

$$\mu_i' = \mu_i'' = \mu_i^\sigma \text{ for all } i \quad (10)$$

We have used the fact that the variations of  $U'$ ,  $U''$ ,  $n_i'$ ,  $n_i''$  and  $V'$  are independent, while those of  $V''$  and  $A^\sigma$  depend on that of  $V'$ . Thus, equilibrium requires that the temperature and the chemical potential of each component shall be uniform throughout the system, and that the two bulk phases differ in hydrostatic pressure by an amount  $\sigma dA^\sigma/dV'$ . A theorem of Gauss states that  $dA^\sigma/dV'$  is equal to the mean curvature of the interface  $C$  (defined as the sum of the reciprocals of the two principal radii of curvature or, alternatively, as minus the divergence of the normal vector). Thus, from (9):

$$p' = p'' + \sigma C \quad (11)$$

a result first stated by Young in 1804 and by Laplace in 1805.

Introducing the surface excess concentration of component  $i$ ,  $\Gamma_i = n_i^\sigma/A^\sigma$ , and the surface excess entropy per unit area,  $s^\sigma = S^\sigma/A^\sigma$ , the Gibbs-Duhem equation for the interface is:

$$0 = S^\sigma dT + d\sigma + \sum \Gamma_i d\mu_i \quad (12)$$

which, for an ideal dilute solution at constant temperature, becomes:

$$\Gamma_i = -\frac{1}{RT} \left( \frac{\partial \sigma}{\partial \ln c_i} \right)_{T, c_j} \quad (13)$$

This relationship, known as the Gibbs adsorption equation, enables the surface excess of any component to be found from experimental measurements of the concentration-dependence of surface tension. It also demonstrates that the isothermal variation of surface tension with solutal concentration is of opposite sign to that of the adsorption of that solute. Thus, in the usual case where components tend to be positively adsorbed at the interface, the surface tension falls with increasing concentration, whereas in an aqueous electrolyte solution, whose interface is depleted of solute, the surface tension increases with increasing concentration.

Equilibrium interfacial configurations, and their stability, will be considered in the following two sections. It is, however, worth noting here the effect of introducing external fields. In a system containing  $k$  distinct interfaces, and

subject to both gravitational and rotational fields, the stable equilibrium configuration is that which minimizes the sum of the energy contributions:

$$\sum \sigma_k A_k + mgz^\theta - (1/2)I\omega^2 = \text{minimum} \quad (14)$$

where  $m$  is mass,  $z^\theta$  is the height of the centre of mass,  $I$  the moment of inertia and  $\omega$  the rotation rate. This condition is directly relevant to the problem of the experimental measurement of surface or interfacial tension, since, with one exception, virtually all methods applicable terrestrially (such as capillary rise, Wilhelmy plate, du Noüy ring, drop volume, drop weight, etc.) depend on a balance between variations of the first two terms of equation (14). In the absence of gravity (or, more generally, at low Bond number) they are inapplicable. The sole exception is the spinning-drop method, in which a strong centrifugal field is used to deform an interface, and variations of the first and third terms are balanced. This is therefore the only practicable method of measuring interfacial tension in orbit. Even this method fails when the density difference between the fluids tends to zero.

#### B.4. Capillary Equilibrium

Fluid static configurations must satisfy the mechanical equilibrium condition:

$$\nabla p + \nabla u = 0 \quad (15)$$

where  $p$  is the hydrostatic pressure and  $u$  is the potential function of any operative body force field. Where a fluid interface is involved, necessary boundary conditions are:

$$p^+ - p^- = \sigma C \quad (16)$$

(Laplace equation), and, at a three-phase line:

$$\sin \theta_1 / \sigma_{23} = \sin \theta_2 / \sigma_{13} = \sin \theta_3 / \sigma_{12} \quad (17)$$

(Neumann's triangle), where the phases are labelled 1, 2 and 3, and  $\sigma$  and  $\theta$  are the interfacial tensions and angles as labelled in Fig. 1.  $C$  is a local mean

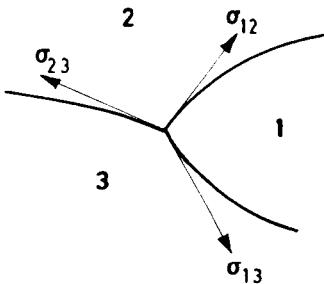


Fig. 1: Confluence of three fluid phases: Neumann's Triangle

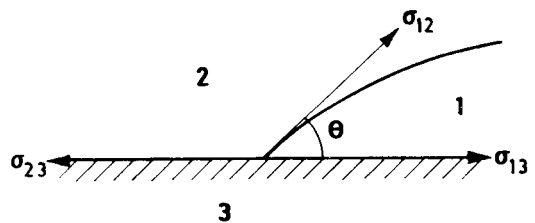


Fig. 2: Fluid interface on a smooth, uniform solid surface: Young's Equation

curvature, and  $p^+$  and  $p^-$  are the hydrostatic pressures on the positively- and negatively-curved sides of the fluid interface. (The mean curvature is defined as  $C = 1/r_1 + 1/r_2$ , where  $r_1$  and  $r_2$  are the principal radii of curvature. The mean curvature is conventionally regarded as positive with respect to the phase within which resides the centre of curvature corresponding to the smaller of the two principal radii.)

When one of the phases is solid and smooth, an energy minimization leads to the conclusion that the fluid interface meets the solid at a characteristic contact angle,  $\theta$ , given by Young's equation (Fig. 2):

$$\sigma_{23} = \sigma_{13} + \sigma_{12} \cos \theta \quad (18)$$

Furthermore, if the solid surface presents a singularity at the three-phase line, either geometrical or chemical (Fig. 3), the contact angle becomes indeterminate in the range (see Fig. 2):

$$\theta_c = \pi - \phi_s \quad \text{or} \quad (19a)$$

$$\theta_c = |\theta_1 - \theta_2| \quad (19b)$$

The resultant anchoring of the three-phase line at the discontinuity, known as canthotaxis, is important for fluid management in microgravity.

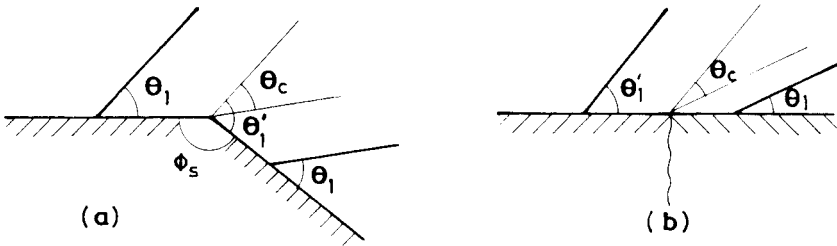


**Fig. 3:** Fluid interface on a solid surface which is (a) rough, and (b) non-uniform in wettability: the phenomenon of canthotaxis

Despite its long history, Young's equation is still the subject of active controversy, first because it involves the two solid surface tensions  $\sigma_{13}$  and  $\sigma_{23}$ , which are not readily susceptible to independent measurement, and secondly because the contact angle in any given system, being peculiarly vulnerable to the effects of surface contamination and of undetected surface roughness, is itself subject to large experimental errors of measurement. (Indeed, it may show large hysteresis between advancing and receding angles, probably as a result of canthotaxis, and in addition may show velocity-dependence when the contact line is in motion, as during spreading).

Early objections to this equation were that its original derivation was based on a resolution of forces (parallel to the solid surface) which act on an imponderable entity, the three-phase line, and that a resolution perpendicular to the

solid surface leaves an unbalanced force of  $\sigma_{12} \sin \theta$  [7]. The second of these arguments is removed by taking into account the elastic strain undergone by the solid near the three-phase line [8]; this argument has been supported experimentally by observations of contact angle on solids of low rigidity modulus, such as mica and gelatine, which show appreciable deformation in the vicinity of the contact line [9, 10]. The first objection was answered by the rederivation of Young's equation from calculation of the virtual work accompanying an infinitesimal displacement of the contact line from its equilibrium position [11]. This not only demonstrated the general thermodynamic validity of the equation, but also showed that it was independent of the action of gravity.

This very important conclusion seems to have gone largely unnoticed, even though it is intuitively reasonable, the contact angle being determined ultimately by intermolecular forces (the balance between cohesive forces within the fluids and adhesive forces between each of them and the solid), which operate over very short distances where differences of gravitational potential are entirely negligible. Nevertheless, there have been reported instances where the wetting behaviour between a melt and its container have shown peculiarities in space, which have been ascribed to microgravity effects.

The problem of capillary equilibrium is thus well-established, and, for capillary surfaces having axial symmetry, and at low values of the Bond number, analytical expressions for the volume enclosed by an interface, the mean curvature and the interfacial area, in terms of either circular or elliptic functions, have been known for a long time [12]. For non-axisymmetric cases, however, the description of equilibrium configurations relies either on numerical computation (e.g. [13–19]), or alternatively on microgravity experiments.

Naturally, a great deal of the earlier work has centred on terrestrial conditions, where the Bond number is significant. Extensive numerical studies have covered most cases of interest in which the gravity vector is parallel to an axis of rotational symmetry, such as sessile and pendent drops and bubbles [14–19]. The results are often non-dimensionalized by division by powers of the capillary length, which becomes infinite as the Bond number tends to zero, and they therefore cannot be readily translated to the microgravity case. For a

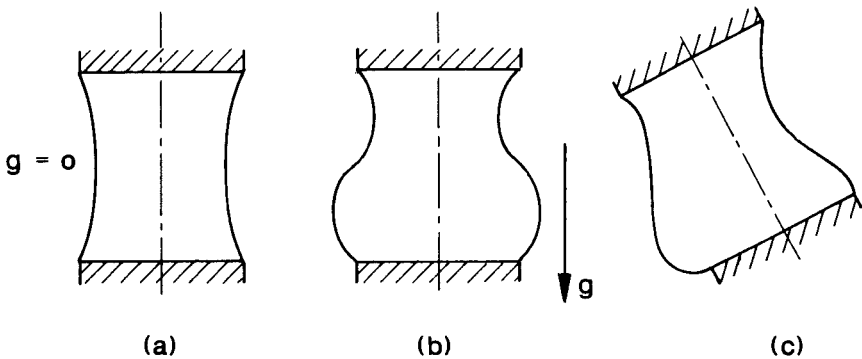


**Fig. 4:** Liquid bridges anchored between equal solid discs, (a) with  $Bo = 0$ , (b) with the gravity vector parallel to the zone axis, and (c) a non-axisymmetric case (diagrammatic)

liquid bridge, i.e. a body of fluid anchored between coaxial circular discs, as in Fig. 4, a more convenient scaling length is the radius of one of the discs. Studies where the gravity vector is otherwise directed, and where axial symmetry is consequently lost, are both rare and approximate [20–22].

Whilst eq. (15) describes the mechanical equilibrium of a system containing a curved fluid interface, its diffusional equilibrium imposes a further requirement, namely, that of uniformity of chemical potential for each component. Since chemical potential is a function of hydrostatic pressure, which in turn is a function of curvature (eq. (16)), the equilibrium concentration of each component in each phase will adjust itself so as to render the chemical potentials uniform throughout the system. The resultant condition for diffusional equilibrium is given by the Kelvin equation, which for an interface between an incompressible liquid and an ideal vapour takes the form:

$$\frac{RT}{v_l} \ln \frac{p}{p^0} = \sigma C \quad (20)$$

where  $R$  = the universal gas constant,

$T$  = absolute temperature,

$v_l$  = molar volume of liquid,

$p^0$  = saturation vapour pressure of bulk liquid (planar interface) at the temperature  $T$ , and

$p$  = saturation vapour pressure over the curved interface.

Thus, a spherical liquid droplet (for which  $C > 0$ ) exerts an enhanced vapour pressure ( $p > p^0$ ). Conversely, a wetting liquid contained in a capillary channel, or forming a small nodoid bridge between two solid spheres, has a negative mean curvature, and consequently exerts a reduced vapour pressure ( $p < p^0$ ). The same is true for a small vapour bubble in a liquid, which can therefore exist in equilibrium only if a reduced pressure, equal to  $p - \sigma C$ , is applied to the liquid. (This pressure may even become negative, so that the liquid phase may be subjected to a tensile force.)

However, the Kelvin effect becomes appreciable only for radii of curvature of  $10^{-6}$  m or less, and is therefore negligible for the macroscopic systems normally studied in microgravity. An analogous form of eq. (20), applicable to the solid/solution interface, is responsible for the enhanced solubility of small crystals, and is relevant to the nucleation of crystal growth from solution; it is, however, unaffected by the absence of gravity.

### B.5. Capillary Stability

The equilibria described by eq. (15) and (20) may be stable, unstable or neutrally stable; stable equilibria may be either absolute or metastable. At zero Bond number, the conditions for stability [23–28] are, for Laplace equilibrium:

$$\left( \frac{\partial^2 A}{\partial \xi^2} \right)_v \geq 0 \quad (21)$$

and, for Kelvin equilibrium,

$$\left(\frac{\partial^2 A}{\partial v^2}\right)_\xi \geq 0 \quad (22)$$

where  $V$  is the volume enclosed by an interface,  $\xi$  is a parameter describing "shape" and  $A$  is an effective area defined by:

$$A = A_{12} - A_{13} \cos \theta \quad (23)$$

$A_{ij}$  being the area of the  $i$ - $j$  interface, as labelled in Fig. 2.

Thus, it follows that a spherical liquid droplet and a sessile liquid drop are both Laplace stable, since a spherical surface presents a minimum area for a given enclosed volume. Both also happen to be Kelvin unstable, though this is not relevant to microgravity experiments, for the reasons given above.

More generally, a surface shape is stable if the second derivative of the total energy  $\sigma A + U$  with respect to all allowed deformations  $\delta \xi$  is positive definite, i.e. if:

$$\left(\frac{\delta^2(\sigma A + U)}{\delta \xi^2}\right)_v > 0 \quad (24)$$

With the first variation vanishing, the second variation  $\delta^2(\sigma A + U)$  becomes a quadratic form in the allowed surface deformations  $\delta \xi$ . It is positive definite if all its eigenvalues are positive. Therefore, in order to prove stability, it is convenient to transform the second variation of the total energy onto main axes and to check whether all eigenvalues are positive.

This transformation yields a second-order eigenvalue equation for an infinite set of mutually orthogonal surface deformations. If one of the eigenvalues vanishes, then a stability limit has been reached.

It can be shown that the differential equation resulting from this eigenvalue equation for zero eigenvalues may also be obtained by allowing for a surface deformation  $\delta \xi$  together with a pressure variation  $\delta p$  in the Laplace equation. A stability limit is therefore encountered if the Laplace equation has two neighbouring solutions with the same liquid volume but differing in pressure. The stability condition [24] may thus be replaced by:

$$\left(\frac{\partial V}{\partial p}\right)_{\text{equilibrium}} = 0 \quad (25)$$

This condition, which is often termed the minimum volume condition, is in fact an extremum volume condition.

The fact that at a stability limit the eigenvalue of the relevant surface deformation changes sign means that numerical methods, such as those based on finite elements or on finite differences, fail to converge. A surface deformation whose eigenvalue is becoming negative increases, rather than decreasing, with iteration. Thus, the instability is reflected in the numerical solution. Naturally, if the numerical method is restricted to axisymmetric deformations, the  $C$ -mode (skipping-rope) instability is not shown up in this way.

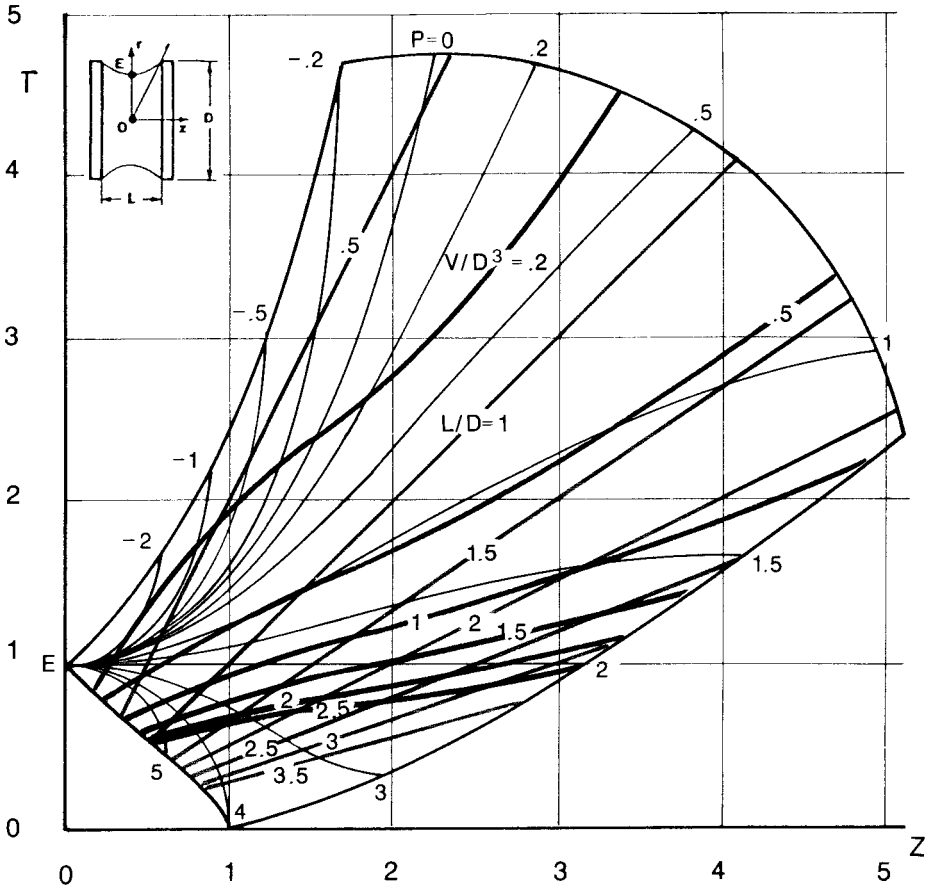
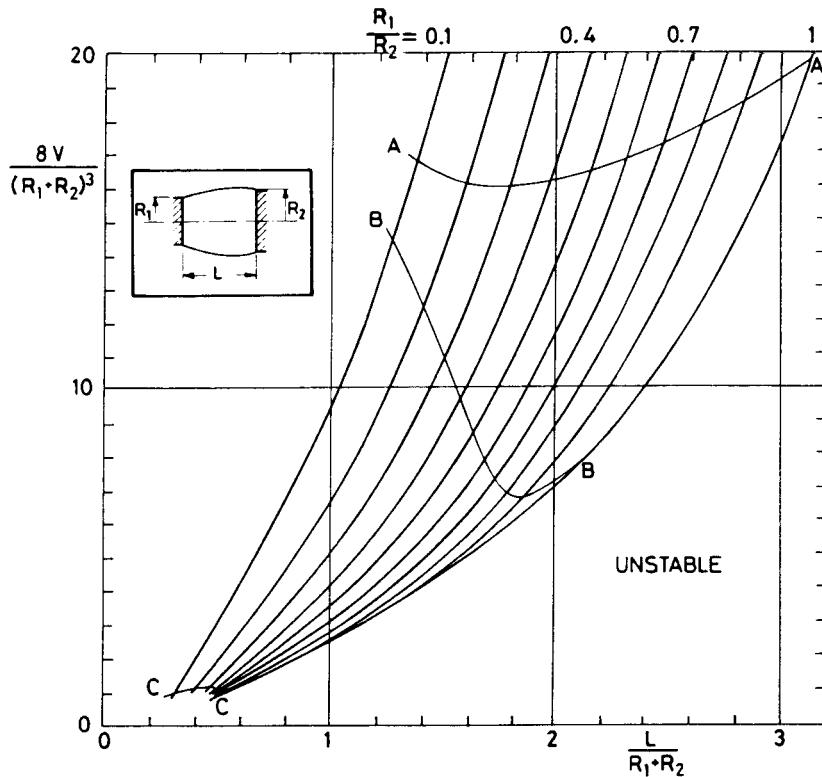


Fig. 5: The black curves show the equilibrium semi-profiles, in  $r$ - $z$  coordinates as defined in the inset, of zero-gravity liquid bridges between circular solid discs of diameter  $D$ , a distance  $L$  apart. Note that  $r$  is scaled so that the equatorial radius  $OE$  is unity. The blue curves are contours of constant  $V/D^3$ , where  $V$  is the volume of liquid contained in the bridge, and the red lines are contours of constant  $L/D$ . To construct a bridge profile of given  $V$ ,  $L$ , and  $D$ , the intersection of the appropriate  $V/D^3$  and  $L/D$  lines is found by interpolation; the bridge will then have the profile passing through that point. Each profile is labelled (in black) with a value of the dimensionless number  $P$ ; the hydrostatic pressure within the bridge then differs from that outside by an amount  $\sigma P/Dr$ . The thick black envelope defines the stability limits: no stable bridges can be formed outside these limits of  $r$  and  $z$ .

A well-known example of Laplace instability concerns a cylindrical fluid interface, which is unstable if its length exceeds its circumference [29]; shorter cylinders are Laplace metastable [30]. A comprehensive summary of Laplace equilibrium conditions for all possible floating zones anchored between equal discs is given in Fig. 5 [31]. The solutions for unequal discs have also been systematically investigated [32] (Fig. 6). Note that the zone length and volume are scaled in terms of the disc radius (or, in the case of unequal discs of radii  $R_1$  and  $R_2$ , in terms of the mean radius  $(R_1 + R_2)/2$ , as a function of the dimensionless parameter  $K = (R_1 - R_2)/(R_2 + R_1)$ .



**Fig. 6:** Stability limits for a zero-gravity liquid bridge of volume  $V$  and length  $L$  held between unequal discs of radii  $R_1$  and  $R_2$ . The parameter  $K$  is defined in the text. For a given  $K$ , the stable bridge volumes and lengths lie to the upper left of the appropriate curve. The loci  $AA$ ,  $BB$  and  $CC$  correspond respectively to bridges with minimum undulation, with local cylindricity at the larger disc, and with catenoidal ( $C = 0$ ) profiles

The sensitivity of such equilibria to small accelerations is potentially important in space applications, where both unsteady (“ $g$ -jitter”) and relatively steady accelerations (e.g. from spacecraft drag and attitude control) may be encountered. The effect of such accelerations on the volume-length stability envelope of liquid bridges is more readily calculable if the acceleration acts along the symmetry axis. The results of such calculations are shown in Fig. 7. Accelerations are expressed in terms of Bond numbers, in order to include the effects of specific fluid properties and of physical dimensions. As a numerical example, an acceleration of  $1 \text{ cm s}^{-2}$  (or  $10^{-3} g_0$ ) applied to a liquid bridge of water of 1 litre volume, gives a Bond number of 1.4. Figure 7 shows that sensitivity to such small accelerations is by no means negligible. For unsteady accelerations, investigation of the frequency-dependence of the response is clearly important.

It may be noted here that alternative methods of achieving low Bond numbers (eq. (1)) encounter comparable difficulties. To obtain  $\text{Bo} = 1.4$  under terrestrial gravity by miniaturization, the volume of water would need to be reduced to  $0.033 \text{ cm}^3$ . On the other hand, application of Plateau’s neutral buoyancy technique to a liquid bridge of water 1 litre in volume, by surrounding

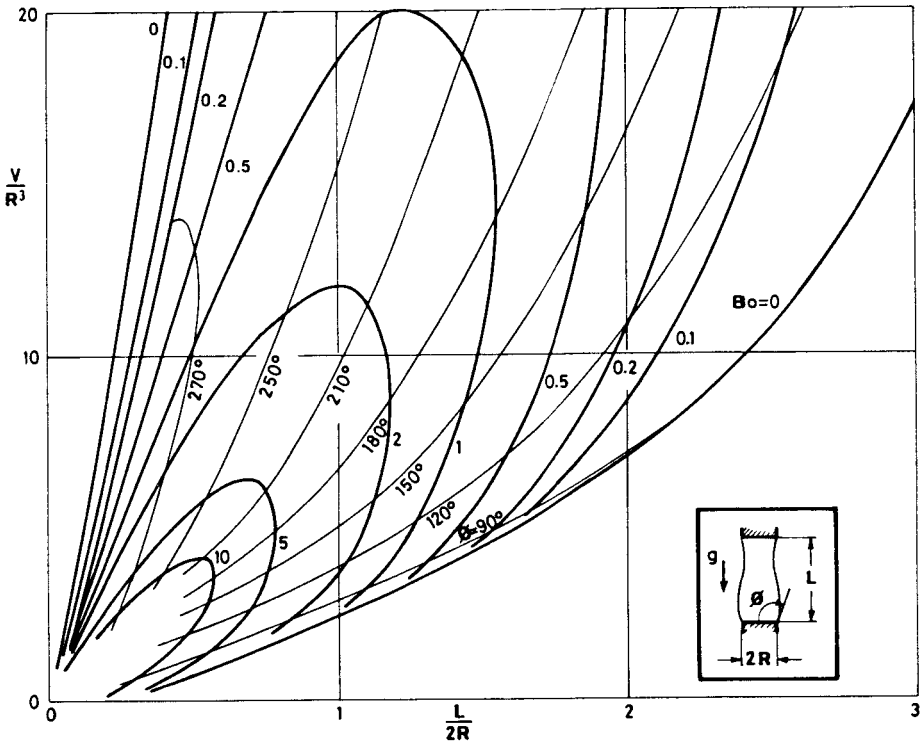


Fig. 7: Stability limits for a liquid bridge of volume  $V$  and length  $L$ , held between equal discs of radius  $R$ , undergoing an axially-directed acceleration such as to produce given values of the Bond number  $Bo = \rho g R^2 / \sigma$ . The angle  $\phi$  is defined in the inset

it with an immiscible liquid of equal density – say an appropriate mixture of dibutyl phthalate and dioctyl phthalate – would require that the densities be matched to about 4 parts in  $10^4$  to achieve the same Bond number. Since the coefficients of thermal expansion of the two liquids will generally be unequal, this demands very careful temperature control.

### B.6. Rotational Stability

A further problem of interest concerns a steadily-rotating fluid held between coaxial end-plates. Skylab experiments [33] demonstrated that this can deform in either axisymmetric or non-axisymmetric modes (described as “amphora” and “C-mode” respectively), as shown in Fig. 8. The relative influence of centrifugal and capillary effects is here described by the Weber (or rotational Bond) number:

$$We = d^3 \omega^2 \Delta \rho / \sigma \quad (26)$$

where  $\omega$  is the angular rotation rate, and  $d$  may conveniently be identified with the radius of the supporting discs. An important practical application is to the process of zone-melting, where the molten zone is usually rotated in order to maintain temperature uniformity.

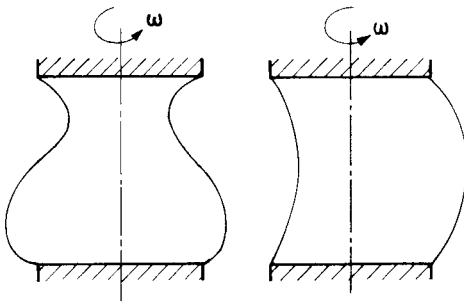


Fig. 8: Amphora and C-mode deformations of a rotating liquid bridge

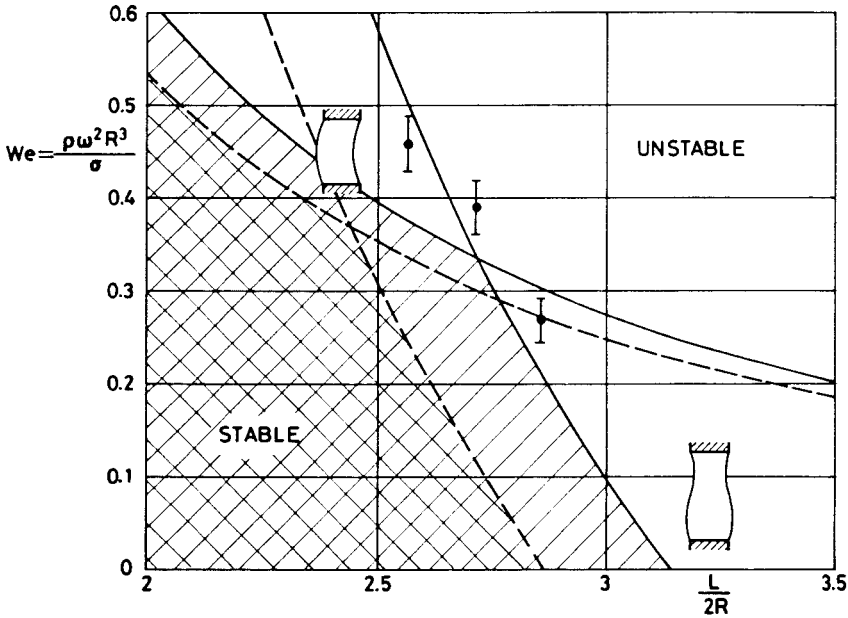


Fig. 9: The full lines show the amphora and C-mode stability limits for an initially cylindrical liquid bridge of length  $L$ , held between equal discs of radius  $R$ , undergoing steady rotation at an angular rate  $\omega$ . The dashed lines show how the stable domain is reduced (cross-hatched area) in the presence of a small axial acceleration corresponding to  $Bo = 0.02$ , as experienced during the D-1 mission. The three experimental points shown were obtained during that flight, each of them producing an amphora-type instability

Theoretical studies [31] have shown that a rotating cylindrical bridge is stable to the two types of deformation for:

$$\frac{L}{2R} < \frac{\pi}{\sqrt{1 + We}} \quad (\text{amphora}) \quad \text{and} \quad (27)$$

$$\frac{L}{2R} < \frac{\pi}{2\sqrt{We}} \quad (C - \text{mode}) \quad (28)$$

A bifurcation therefore occurs at  $L/(2R) = \pi\sqrt{3}/2 \approx 2.721$ . Their respective fields of stability are delineated by the full lines in Fig. 9.

The problem of “spin-up”, in which momentum is being transferred between the supporting disc(s) and the fluid, as the latter approaches solid-body rotation, is of great interest. It has been the subject of much theoretical and experimental studies [34], but lies outside the scope of the present chapter.

Whereas the preceding paragraphs dealt with a rotating fluid mass anchored between two solid discs, the equilibrium and stability of an isolated rotating fluid body is of classical interest [35], since it has been used as a model of stars and galaxies and, at the other extreme, in development of theories of nuclear fission and fusion. Results of recent microgravity experiments dealing with this problem will be discussed in Section C.2.

### B.7. Critical Wetting

The behaviour of the fluid/fluid/solid contact line acquires even greater interest when the two fluids approach a critical point [36]. For a single-component system, this state is the critical point itself, whereas for liquid/liquid systems of more than one component it is the consolute point. It has been predicted theoretically that as this state is approached, the contact angle will tend to zero: one of the two fluid phases will become completely wetting and the other completely non-wetting [37]. At the same time, the thickness of the fluid interface will increase, the transition from one fluid to the other being spread out over a greater distance. This does not, of course, imply an increase in the range of intermolecular forces, but arises rather from a stronger correlation between the fluctuations of density, of thermal origin, which occur naturally in any phase, as the two fluid phases become more nearly identical.

This has important implications for the observation of near-critical systems in terrestrial laboratories. The vertical gradient of fluid density in a gravitational field assumes crucial importance near a critical state, where the compressibility of the fluid tends towards infinity. This cannot be overcome merely by using a working chamber of small vertical height, because of the simultaneous divergence of the correlation length for density fluctuations, which may exceed the dimensions of any terrestrial experimental container before the critical point is attained. It is therefore impossible, in any terrestrial experiment, to attain uniquely the true critical state. Experiments on critical phenomena are, therefore, prime candidates for space flight and several have been proposed. These mostly fall outside the remit of the present chapter (see Chapters VI and VII); it should, however, be noted that critical wetting phenomena may strongly influence capillary behaviour of liquids in microgravity. This is of particular relevance to the solidification of heterogeneous mixtures.

### B.8. Charged Interfaces

A boundary between phases is often characterized by a non-uniform distribution of electrical charge. This can modify the capillary behaviour of the system, in regard both to equilibrium and to stability, by adding to the body forces acting on it.

Such charge may be either static or dynamic in origin. Thus, the adsorption of charged (ionic) species at an interface leads naturally to the formation

of a stable equilibrium electrical double layer (EDL) [38]. Forces between such double layers have a profound effect on colloid stability. On the other hand, relative motion between a dielectric fluid containing charge carriers and a solid surface can generate quite large electrostatic charges, which will tend to concentrate at any free liquid surface and to interact with any other charged surface in the vicinity. When flow ceases, there is a subsequent migration of the charge carriers, with a characteristic relaxation time, tending eventually to depolarize the system.

Whereas a capillary surface under the sole influence of surface tension must adopt a configuration of uniform mean curvature ("homoclastic" surface), a charged interface in a potential gradient will assume a modified configuration. This is still an equipotential surface, but there are now both capillary and electrical contributions to the total potential, and the mean curvature is no longer uniform. Thus, it has been predicted [39] that an initially spherical drop attached to a solid surface will become conical when charged and placed in an electric field.

## C. Results of Previous Microgravity Experiments

Between the early 1970's and the mid-1980's, numerous microgravity experiments relating to capillary phenomena have been flown, both manned and unmanned. Some have been designed specifically for such objectives, while other observations have been incidental – or even accidental – results of experiments in other fields.

The results of many experiments have been outlined at several post-mission conferences [40–43].

Within the confines of this book, we limit ourselves almost entirely to discussion of West European experiments, whilst recognizing, of course, the extensive parallel and independent contributions from US and Soviet experimenters. (We remark in passing that co-ordination between the various nationally-based research efforts in this field, as in other microgravity work, is still largely rudimentary. The scope for global collaboration is great, potentially fruitful, but sadly unfulfilled). We also concentrate on capillary statics rather than dynamics (Chapter III), though the distinction is not always clear.

### C.1. Static Equilibrium and Stability

Following the fluid science demonstration experiments of Skylab [33], a more systematic study of liquid bridge stability has been conducted in the Fluid Physics Module [43, 45]. Various paths have been traversed in the stability diagram of Fig. 5, whereby an instability has been approached either by lengthening a bridge at constant volume, or by depleting a bridge at constant length. The observations tended to confirm the theoretical predictions. Though to some extent hampered by experimental problems the asymmetric breaking predicted from Fig. 5, the progressive acceleration of rupture as the fluid interface adopts an increasingly non-uniform mean curvature was clearly demonstrated. The

formation of a satellite drop and the inertial distortion of the two residual anchored portions of fluid, which ultimately become spherical when quiescent, was also observed.

There have by now been numerous observations of this kind in microgravity, and it is noticeable that the satellite drop always acquires a residual velocity, with both axial and radial components. This probably arises from slight departures from symmetry in the fluid flow immediately preceding rupture of the bridge. Sometimes this motion leads to a collision between the satellite drop and one of the two anchored drops. This collision is almost invariably quasi-elastic, the droplet being apparently specularly reflected. This could result either from electrostatic forces, or from viscous resistance in the thin film of air being displaced from between the drop surfaces. A related observation is that when the two principal residual drops are brought together, they often show marked reluctance to merge, even when they are pressed together so firmly that they become perceptibly non-spherical.

The subject of non-axisymmetric capillary equilibria and their stability has not been investigated systematically. Terrestrially, it is a familiar observation that a wetting fluid which partially fills a rectangular container can adopt various equilibrium configurations (some of which are metastable), as illustrated in Fig. 10. If, on the other hand, the contact angle is large enough to produce a positive curvature in a liquid fillet confined along an interior edge of the container, as in Fig. 11, a modified Rayleigh-type instability can induce separation into discrete droplets. Configurations such as these are clearly relevant to problems of propellant management in liquid fuel tanks. Calculated solutions are very difficult, involving the application of rigorous stability theory [27] to configurations that can be described only by numerical approximations [19, 46, 47]. As yet, however, few microgravity experiments have addressed such problems directly, even though there are strong indications of the existence of interesting phenomena. For example, experiments in aircraft flying parabolic trajectories

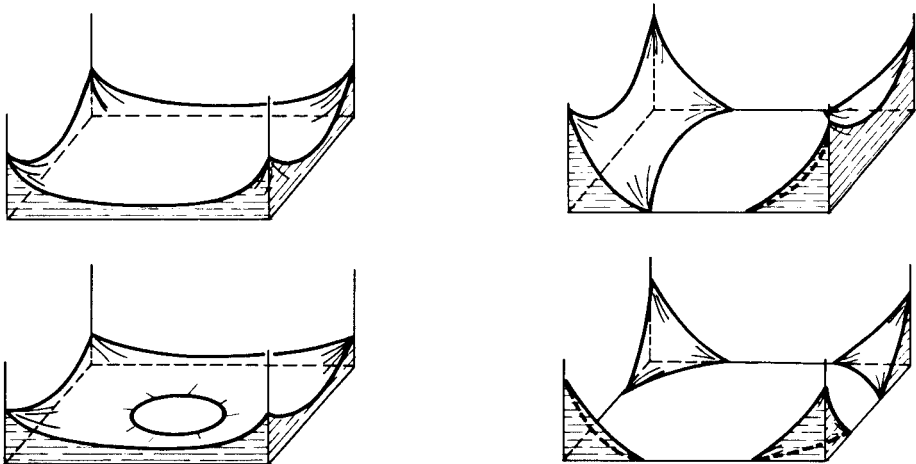


Fig. 10: Various alternative distributions of a small volume of liquid in a rectangular box

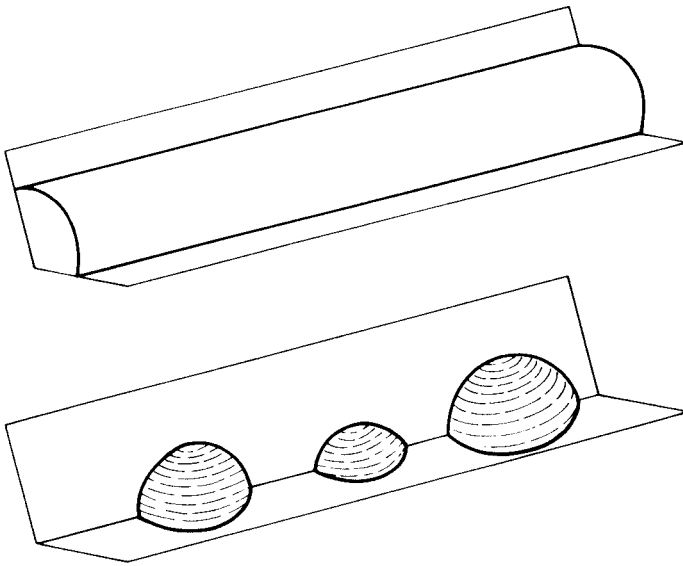


Fig. 11: Instability of a part-cylindrical liquid fillet contained in the internal edge of a box

[48] have demonstrated that an annular ring of water formed around a cylindrical solid support in microgravity can break into three symmetrically-disposed drops (Fig. 12). This nodoidal instability is analogous to the Rayleigh cylindrical instability, and presumably depends on the (circular) length of the ring and its diameter, but has not yet been analysed theoretically.

An experiment on SL-1 [49] was intended to define the stability limits and the volume - curvature relationship for a non-axisymmetric liquid lens held by capillarity in the central space between three solid spheres. This case is of interest as a model of hysteresis in the capillary retention of liquids in porous media, and is relevant to practical problems in soil physics, oil production from underground reservoirs, drying of powders, and so on. Unfortunately, a hardware failure during the mission prevented acquisition of full quantitative data, though an improvisation by the payload specialist enabled some interesting observations to be made. These included the unexpectedly persistent stability of a thin film of the working fluid (a silicone oil) across the central space between the spheres. This was almost certainly due to contamination of the oil, and underlines the need for a careful choice of working fluids and for the scrupulous maintenance of clean conditions in all experimental studies of interfacial phenomena.

## C.2. Rotation and Oscillation

The stability limits of rotating liquid bridges between equal discs were studied on the D-1 mission [45]. Bridges of three different slenderness ratios were accelerated from rest at 9 rmp/minute until breakage occurred. The three slen-

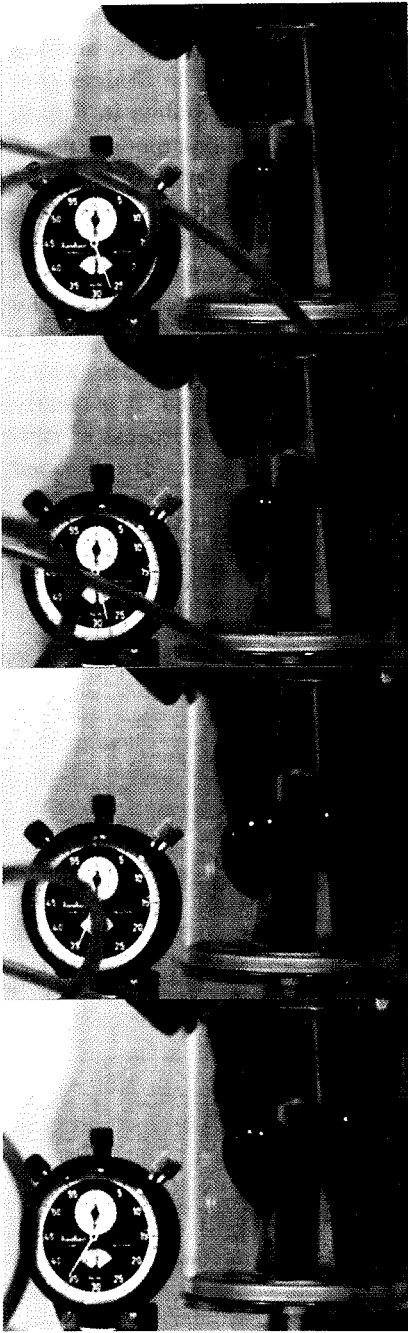


Fig. 12

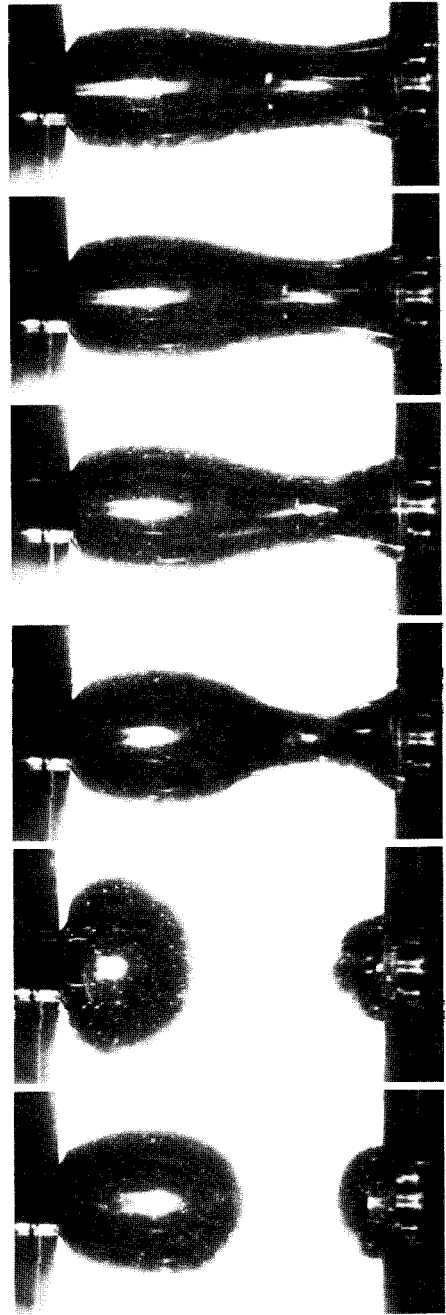


Fig. 13

**Fig. 12:** Instability of a nodoidal liquid ring surrounding a solid cylinder

**Fig. 13:** Breaking sequence of a 100 mm long cylindrical liquid column of silicone oil, rendered unstable by rotation. Times relative to the first frame are 0, 40, 46, 48 and 50 seconds. Bright dots are tracer particles. Note the asymmetric breaking, and (in the final frame) the formation of a satellite drop and the transiently non-spherical shape of the two remnant drops

derness ratios were chosen so that the shortest and longest bridges would be expected to undergo *C*-mode and amphora instabilities, respectively, and the intermediate one lay very close to the expected bifurcation. The bridges chosen for examination are indicated by the three experimental points in Fig. 9. Despite expectations, however, all three broke in the amphora mode, and at rather higher Weber numbers than predicted. The first observation may be attributed to the slight residual acceleration experienced on board Spacelab. Figure 9 shows (dashed lines) the effect of a small axial acceleration ( $Bo = 0.02$ ): the stable region is reduced, and the destabilization is more marked towards amphora-type deformations. The delayed instability may have been caused by the finite viscosity of the working fluid, and the rather rapid spin-up. Figure 13 shows selected frames from the breaking sequence of the longest bridge, which occurred when a rotation rate of about 10 rpm had been attained. It is clearly shown that once the point of instability has been reached, the process of rupture evolves relatively rapidly. The final frame shows the satellite drop formed during rupture.

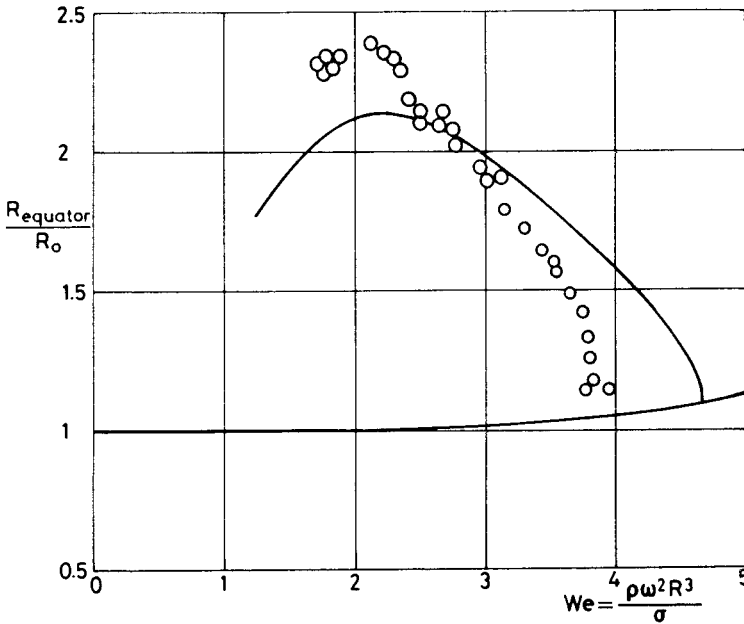
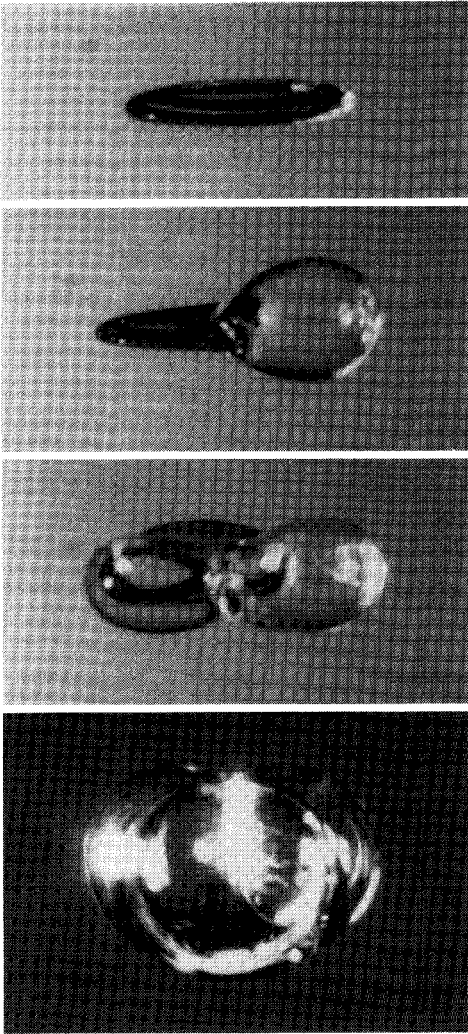


Fig. 14: Calculated and experimental stability limits for an isolated rotating liquid drop [50]

The rotational stability of an isolated liquid drop has been investigated on the SL-3 mission, using an acoustic levitation chamber [50]. An initially spherical drop became increasingly oblate as it was rotated more rapidly (increasing Weber number). Eventually, a two-lobed non-axisymmetric deformation was observed, in accordance with theoretical prediction (Fig. 14). Similar deforma-



**Fig. 15:** Observed break-up of a water drop acoustically levitated on the ground. With increasing levitation power diagonal and trigonal shapes arise

tions have been observed with water drops acoustically levitated on the ground, when the levitating power was successively increased (Fig. 15).

The oscillatory behaviour of tethered drops and of liquid bridges has been studied at low Bond number, both terrestrially (using liquids of matched density) [51], and in space [52]. Some results of the former kind are illustrated in Fig. 16, showing the frequency response of two liquid bridges of different aspect ratio. Although the interpretation of such isopycnic simulation experiments is complicated by viscous and inertial effects in the outer surrounding liquid, the results nevertheless show clearly that the vibrational response has well-defined resonant frequencies, whose values depend on the aspect ratio of the bridge. Comparable experiments on the oscillation of tethered drops, conducted both isopycnically and in genuine microgravity, suggested that interfering effects of the outer liquid were small [52].

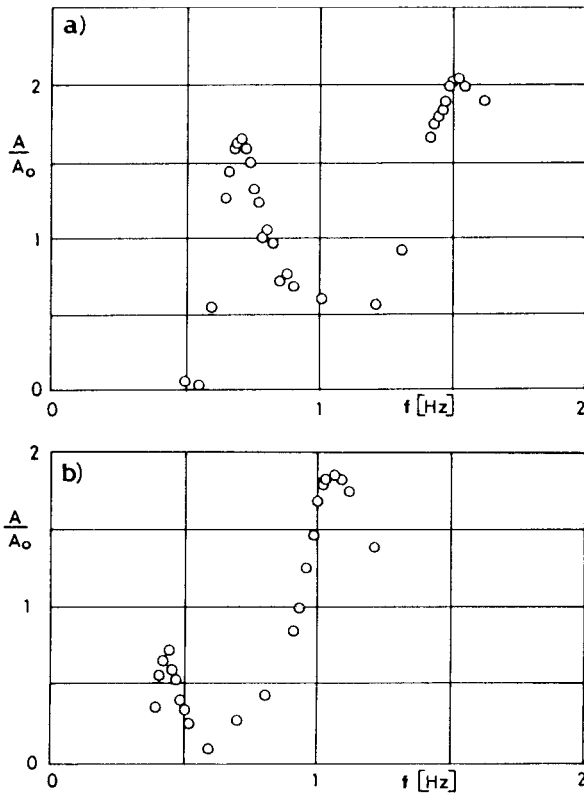


**Fig. 16:** Ratio of deformation amplitude  $A$  to excitation amplitude  $A_0$  versus excitation frequency  $f$  for liquid bridges of silicone oil (having a dynamic viscosity of  $2 \times 10^{-5} \text{m}^2 \text{s}^{-1}$ ) surrounded by a second, density-matched, liquid.  $A_0 = 1.3 \text{ mm}$ . (a)  $L/D = 1.5$ , (b)  $L/D = 1.8$  [51]

### C.3. Critical Wetting

The phenomenon of critical wetting has been observed in several microgravity experiments. For instance [53], on the D-1 mission, a liquid bridge of benzyl benzoate was formed within a surrounding bridge of paraffin oil (both liquids being mutually saturated). This system exhibits a miscibility gap, with an upper consolute temperature of  $47^\circ\text{C}$ . When one of the supporting discs was heated to  $60^\circ\text{C}$ , the benzyl benzoate bridge spread across it, eventually depleting the bridge to the point of capillary instability (Fig. 17).

These observations are strongly relevant to space experiments on melting and resolidification of binary alloy systems with a miscibility gap, since they demonstrate the way in which the spatial distribution of the phases may be determined overwhelmingly by wetting behaviour and by capillary instabilities. When, during cooling of an immiscible alloy under microgravity conditions, the miscibility gap is reached, it is very likely that phase separation will begin at the crucible wall: the component with the lower interfacial tension against the crucible material will precipitate there preferentially. Heterogeneous nucleation

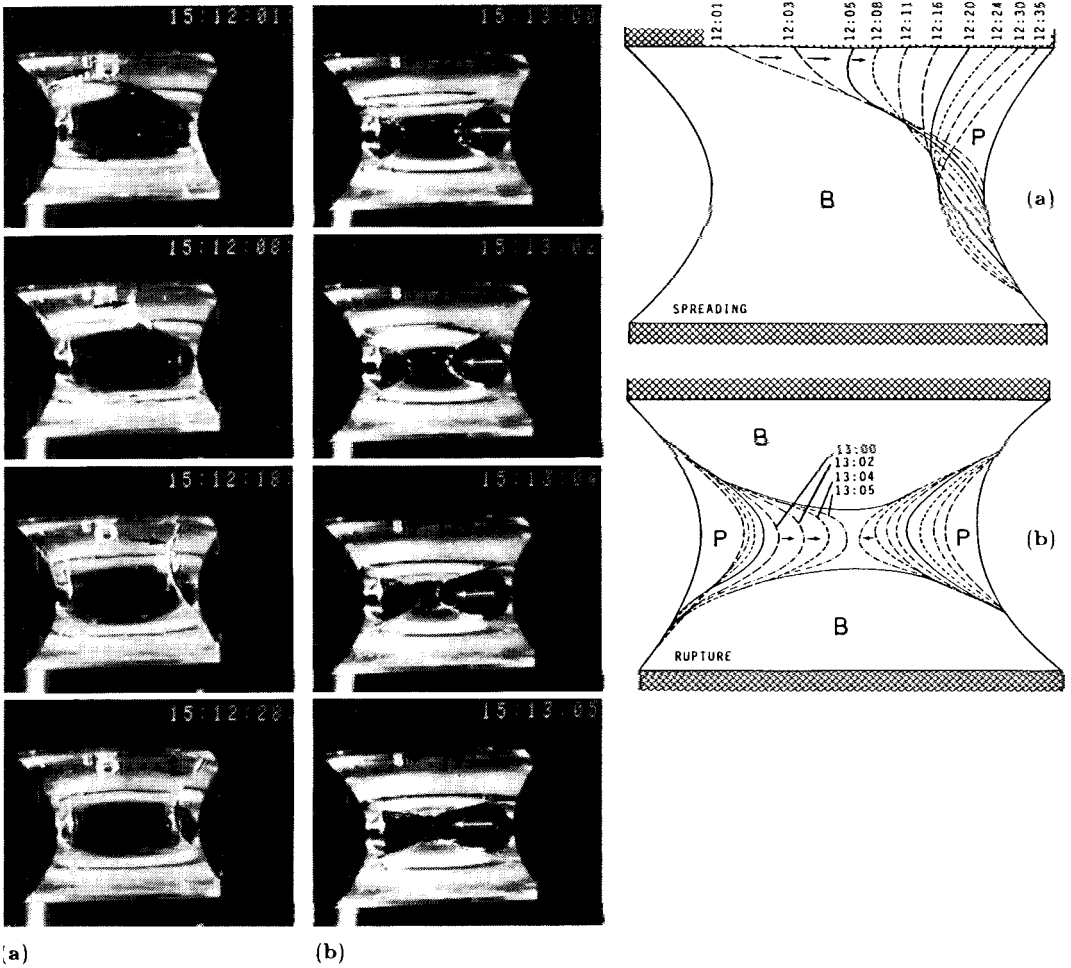


**Fig. 17a,b:** Spreading, and subsequent rupture, of a liquid bridge, brought about by the induction of critical wetting by heating one of the supporting discs to above the consolute temperature (system paraffin oil/benzyl benzoate) [53]

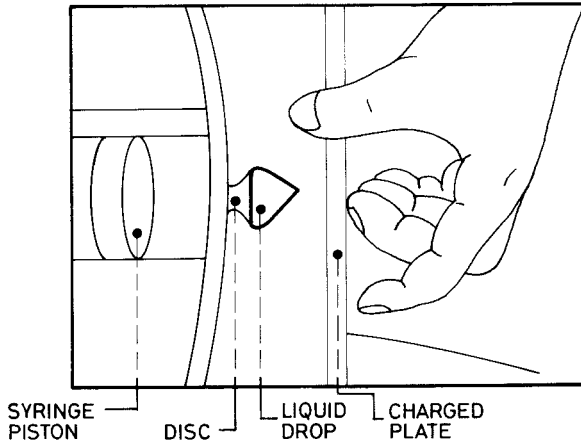
at the wall thus requires less energy than homogeneous nucleation in the bulk melt. Close to the consolute point, the contact angle of one of the components against the crucible material vanishes. This component will therefore spread along the crucible wall, having nucleated there. This effect will be even more marked at the crucible's edges. Capillary forces and spreading conditions thus contribute essentially to the phase separation process of immiscible alloys in microgravity.

#### C.4. Charged Interfaces

Although there have so far been no space experiments directed specifically towards this topic, a number of illuminating observations have been recorded. For instance, one experiment flown on STS-5 [54] was designed to investigate the kinetics of spreading of a liquid (di-n-octyl phthalate) on a solid surface



**Fig. 18:** Conical shape of an electrified liquid drop attached to a circular disc, as seen during the STS-5 mission [54]



(Perspex, or Lucite). When the protective cover was stripped off the Perspex sheet, however, a static charge was generated thereon, and, on presentation of the tethered drop of liquid to the solid surface, an immediate reaction was observed between them. The drop, of about 2.5 cm diameter, detached itself from its solid support and leapt across the intervening space of about 10 cm to attach itself, and spread, on the Perspex plate. Meanwhile, the remaining tethered portion of the drop adopted the conical shape predicted by Taylor [39], as shown in Fig. 18, and developed a pulsatile instability at its tip, from which droplets were periodically ejected towards the charged plate.

An example of similar behaviour was seen when the liquid had become accidentally contaminated with bubbles of air during subsequent manipulations. As this liquid was injected into the working space through a small orifice in a Teflon plate, electrokinetic charging of the bubbles occurred. The drop thereby acquired a bulk charge, which caused it to take up an accurately conical shape, once again ejecting fluid at regular intervals from its tip.

## D. Future Prospects

### D.1. Present Interests

The capillary behaviour of fluids in microgravity is likely to continue to be a major research area, both terrestrially and in space. The experimental programme is expected to address both fundamental and applied aspects, with the latter being largely generated by problems in crystal growth and composite materials (where the interaction of capillary and fluid dynamic phenomena is most important).

Investigations of the equilibrium and stability of non-axisymmetric interfacial configurations are likely to be further developed, both in support of theoretical calculations and in order to provide empirical information for design of propellant management devices.

### D.2. Topics to be Addressed in the Future

Present experience of microgravity fluid science, though still rudimentary in many ways, has provided numerous incidental observations, of which some have been described earlier in this chapter, and which suggest fruitful areas for future research.

Critical wetting phenomena have already been mentioned, and are of basic importance in some types of crystal growth experiments. However, the critical wetting experiment described in Section C.3 above [53] poses an intriguing question. As described, critical spreading on one of the plates led to a Rayleigh-type instability of the bridge, which ruptured; yet, had the system been truly at its consolute point, the interfacial tension (which provides the driving force for rupture) would have been zero. Thus, we are led to consider the problem of capillary stability at extremely low values of interfacial tension. This is potentially relevant not only to some types of crystal growth and phase separation in general, but also to enhanced oil recovery processes in which surfactants are used to reduce the interfacial tension between oil and brine to extremely low values [55].

A novel proposal [56] is to study adsorption at the solid/fluid interface, in microgravity, of near-critical single-component fluids (e.g. SF<sub>6</sub> on graphitized carbon black). Terrestrial experiments [57, 58] have shown a logarithmic divergence of surface excess as the critical temperature is approached at constant fluid density. Study of this so-called "critical adsorption" yields fundamental information on critical exponents (see Chapter VI). Although the phenomenon itself is gravity-independent, its experimental study is not so, because of the density gradient induced by gravity in the experiment chamber (cf. Section B.7).

Observations of the effect of electrostatic charge on interfacial behaviour (Section C.4) suggest that more systematic investigation, both of the production of such charge and of its effects, would be worthwhile. Another opportunity offered by microgravity is that of studying the charge distribution at the liquid/vapour interface by measurements of bubble electrophoresis. Terrestrially, such measurements are applied very widely to the solid/liquid interface, and

have provided a wealth of useful information, but experiments on bubbles are impeded by the instability of small bubbles and the buoyancy of larger ones.

The stability of foams depends on interaction between electrical double layers at the opposing surfaces of thin liquid films, and on the rate of drainage of liquid from such films; the latter is both gravity-induced and driven by gradients of capillary pressure between the flat film and the negatively-curved triple junctions (Plateau borders) between contiguous films [59]. There is evidence [60] for the existence of a "contact angle" (i.e. a discontinuity of surface gradient) between the film and its border. Microgravity offers the possibilities of separating gravity and capillary effects, and of studying films of large physical dimensions.

The sensitivity to weak forces of large liquid bridges in microgravity has also been exploited in an ingenious attempt to measure the disjoining pressure in relatively thick liquid films spread on solids. By forming catenoidal bridges, whose interfacial curvature is zero and which therefore generate no capillary pressure, and by using an end-plate in the form of a very shallow cone, it is in principle possible to extend by several orders of magnitude the range of film thicknesses accessible to terrestrial experiments. The experiment is, however, a demanding one, and when flown on SL-1 yielded inconclusive results [61]. A second attempt, flown on the D-1 mission, appears to have been more successful, but no results relating disjoining pressure to film thickness from this experiment have yet been published. If this method is successful, however, it is likely to be much more fully exploited in later missions, since it addresses the very fundamental question of the nature of long-range intermolecular forces.

### D.3. General Remarks

An example of the interaction which exists between the present programmes in fluid physics and in crystal growth is shown in Fig. 19 [62]. Zone melting of silicon is a process of considerable interest in the microgravity materials science effort. Knowledge gained from studies of capillary behaviour in microgravity has made it possible to predict theoretically the boundary between stable and unstable growth conditions in this system, and hence to define appropriate parameters for stable growth. At their present stage, these calculations do not take full account of such complicating factors as Marangoni convection, rotational instabilities, and wetting phenomena. However, as seen here and in Chapter V, these are already the subject of much active research, and we can anticipate a much more complete understanding of all aspects of fluid physics related to crystal growth processes.

This point provides a clear illustration of the role of capillary studies in the microgravity programme. On the one hand these have considerable fundamental significance, and the advent of opportunities for basic research using manned space platforms is enabling the continued growth and extension of a body of knowledge first begun more than a century ago. On the other hand, a proper understanding of capillary phenomena is essential for the development and exploitation of materials processing in microgravity, as well as for general questions of on-board fluid management.

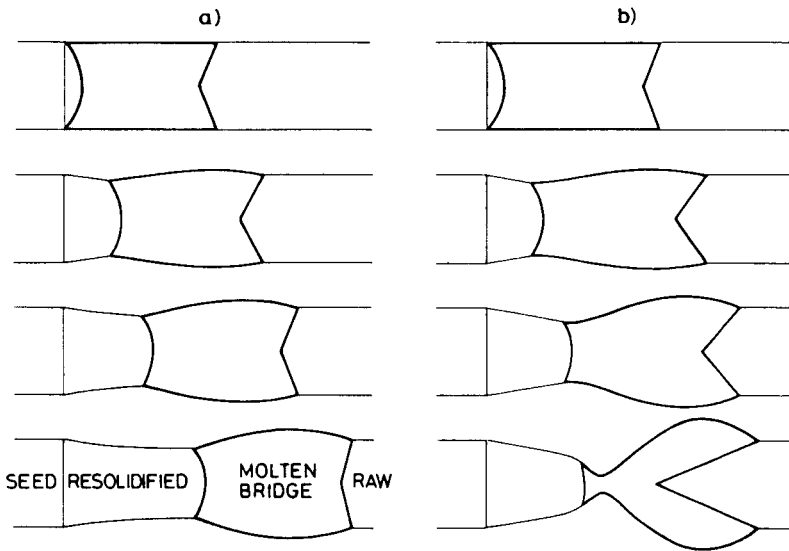


**Fig. 19:** Theoretically-predicted shapes of the molten zone of an initially cylindrical silicon rod, assuming constant melt length, for two different furnace powers: (a) stable, and (b) unstable growth [63]

We believe that our limited experience of capillarity in microgravity has already produced results of much interest, both fundamental and applied, and both from space experimentation itself and from the ground-based work which it has stimulated. The topic has considerable future potential, evidently; but for this to be adequately and efficiently fulfilled, certain conditions can be stated.

Improved experimental facilities in space are an urgent necessity, especially in regard to fluid management and to shape visualization and analysis. The potential for real-time on-board shape analysis, using video-based image analysis techniques, should be pursued, as a means both of improved experiment control and of more rapid assessment of results. The choice of working fluids in space will, we hope, be freed from over-protective safety constraints.

In particular, the inertial effect during injection into a spherical drop (“jetting”) appears to have been underestimated. On the other hand, the ease of achieving canthotaxis at an undercut disc edge, even when supplemented by a supposed “anti-spread” barrier, was seriously overestimated.

Improved collaboration between experimenters, on both interdisciplinary and international levels, is greatly to be desired. The present IWG system within ESA is exemplary, but too limited in scope. More assistance is also needed for ground-based theoretical and experimental work, and a coordination link should be established for this purpose.

Above all, it should be recognized that close interaction between the ground-based experimenter and his space counterpart, and opportunities for frequent iteration of experiments, are two key factors for success, not only here but in all areas of space research.

These are, we hope, the opportunities that we can bequeath to our successors in the next century.

## F. References

1. Watts W., British Patent 1347, December 10, 1782
2. Plateau J.A.F., *Statique expérimentale et théorique des liquides soumis aux seules forces moléculaires*, Gauthiers-Villars, Paris, 1873
3. Gibbs J.W., *Collected Works*, Longmans Green, New York (1928); Dover reprint, New York, 1961. (The original formed part of a lengthy paper, "On the equilibrium of heterogeneous substances", appearing in several issues of *Trans. Connecticut Acad. Sci.*)
4. Van der Waals J.D., Thesis, *Over de Continuïteit van den Gasen, Vloiestoetstand*, Leiden, 1873. See also Rowlinson J.S., *Nature* **244**, 414 (1973)
5. Evans R., *Mol. Phys.*, **42**, 1169 (1981)
6. Rowlinson J.S. and Widom B., *Molecular Theory of Capillarity*, Clarendon Press, Oxford, 1982
7. Bikerman J.J., *Proc. 2nd Int. Cong. Surf. Activity*, **3**, 125 (1957), and discussion, pp. 187-190
8. Lester G.R., *J. Colloid Sci.*, **16**, 315 (1961)
9. Tabor D. and Bailey A.I., *Proc. 2nd Int. Cong. Surf. Activity*, **3**, 189 (1957)
10. Michaels A.S. and Dean S.W., *J. Phys. Chem.*, **66**, 1790 (1962)
11. Johnson R.E., Jr., *J. Phys. Chem.*, **63**, 1655 (1959)
12. Clerk Maxwell J., *Encyclopaedia Britannica*, 9th Ed., Vol. 5, p. 56; Adam & Charles Black, Edinburgh, 1875
13. Bashforth F. and Adams J.C., *An attempt to test the theories of capillary action*, University Press, Cambridge, 1883
14. Fordham S., *Proc. Roy. Soc.*, **A 194**, 1 (1948)
15. Padday J.F., *Trans. Roy. Soc. London*, **A 269**, 265 (1971)
16. Boucher E.A. and Evans M.J.B., *Proc. Roy. Soc.*, **A 346**, 349 (1975)
17. Hartland S. and Hartley R.W., *Axisymmetric fluid-liquid interfaces*, Elsevier, Amsterdam, 1976
18. Orr F.M., Scriven L.E. and Rivas A.P., *J. Fluid Mech.*, **67**, 723 (1975)
19. Langbein D., in *Materials Sciences in Space*, Eds. Feuerbacher B., Hamacher H. and Naumann F.J., Springer, 1986, p. 401
20. Lomas H., *J. Colloid Interface Sci.*, **33**, 548 (1970)
21. Princen H.M., *J. Colloid Interface Sci.*, **36**, 157 (1971)
22. Wolfram E. and Faust R., in *Wetting, Spreading and Adhesion*, Ed. Padday J.F., Academic Press, London, 1978
23. Pitts E., *J. Fluid Mech.*, **63**, 487 (1974)
24. Everett D.H. and Haynes J.M., *Z. phys. Chem. (N.F.)*, **97**, 301 (1975)
25. Majumdar S.R. and Michael D.H., *Proc. Roy. Soc.*, **A 351**, 89 (1976)
26. Boucher E.A., Evans M.J.B. and Kent H.J., *Proc. Roy. Soc.*, **A 349**, 81 (1976)
27. Erle M.A., Gillette R.D. and Dyson D.C., *Chem. Eng. J.*, **1**, 97 (1970)
28. Dyson D.C., *Prog. Surface and Membrane Sci.*, **12**, 479-568 (1978)
29. Lord Rayleigh, *Proc. Roy. Soc.*, **29**, 71 (1879)
30. Haynes J.M., *J. Colloid Interface Sci.*, **32**, 652 (1970)
31. Da Riva I. and Martinez I., *Proc. 3rd Europ. Symp. Mats. Sci. Space*, ESA SP-142, 67 (1979)
32. Martinez I., *Proc. 4th Europ. Symp. Mats. Sci. Space*, ESA SP-191, 267 (1983)
33. Carruthers J.R., Gibson E.G., Klett M.G. and Facemire B.R., *AIAA Paper 75-692* (1975)
34. Benton E.R. and Clark A., *Ann Rev. Fluid Mech.*, **6**, 257 (1974)
35. Chandrasekhar S., *Proc. Roy. Soc.*, **A 286**, 1 (1965)
36. Cahn J.W., *J. Chem. Phys.*, **66**, 3367 (1977)
37. Moldover M.R. and Cahn J.W., *Science*, **207**, 1073 (1980)
38. See, e.g., Kruyt H.R., *Colloid Science*, Elsevier, New York, 1952; Spaarnay M.J., *The Electrical Double Layer*, Pergamon, New York, 1972
39. Taylor G.I., *Proc. Roy. Soc.*, **A 280**, 383 (1964)
40. Siebel M.P.L. (Ed.), *The Third Skylab Mission: Skylab Results*, NASA, 1974
41. *Proc. 4th European Symp., Materials Science under Microgravity*, Madrid, 5-8 April 1983; ESA SP-191, 1983
42. *Proc. 5th European Symp., Materials Science under Microgravity*, Schloß Elmau, 5-7 November 1984; ESA SP-222, 1984

43. XXXIII IAF Congress, Paris, 1982
44. Martinez I., Ref. 42, p. 31
45. Da Riva I. and Martinez I., *Naturwissenschaften*, **7**, 345 (1986)
46. Orr F.M., Scriven L.E. and Rivas A.P., *J. Colloid Interface Sci.*, **52**, 602 (1975)
47. Orr F.M., Scriven L.E. and Chu S., *J. Colloid Interface Sci.*, **60**, 402 (1977)
48. Langbein D., unpublished KC-135 observations
49. Haynes J.M., *Materials Science in Space*, ESA SP-114, 467 (1976)
50. Wang T., as quoted in D. Dooling, **SL-3 Data**, Commercial Space, Winter 1986, p. 73
51. Sanz A., *J. Fluid Mech.*, **156**, 101 (1985)
52. Rodot H. and Bisch C., Ref. 42, p. 23
53. Langbein D. and Heide W., *Proc. 6th European Symp., Materials Science under Microgravity*, Bordeaux, 2-5 December 1986, p. 117-123
54. Allen J.P. and Haynes J.M., unpublished observations
55. Slattery J.C., *Am. Inst. Chem. Eng. J.*, **20**, 1145 (1974)
56. Findenegg G.H., Ref. 41, p. 385
57. Specorius J. and Findenegg G.H., *Ber. Bunsenges. phys. Chem.*, **84**, 690 (1980)
58. Loring R. and Findenegg G.H., *J. Colloid Interface Sci.*, **84**, 355 (1981)
59. Mysels K.J., Shinoda K. and Frankel S., *Soap Films, Studies of their Thinning, and a Bibliography*, Pergamon, New York, 1959
60. Mysels K.J., *J. Electroanal. Chem. Interf. Electrochem.*, **37**, 23 (1972)
61. Padday J.F., ref. 42, p. 9
62. Martinez I., unpublished results